

Validation of a Flow Channel to Investigate Velocity Profiles of Friction-Reducing Ship Coatings

J. Weisheit, V.E. Schneider, J.M. Serr, N. Hagemeister & J. Oeffner
Fraunhofer Centre for Maritime Logistics and Services CML, Hamburg, Germany

ABSTRACT: Reducing friction with specialised hull coatings or air lubrication technologies has a potential reducing energy consumption and emissions in shipping. The EU project AIRCOAT combines both by developing a passive air lubrication technology inspired by nature that is implemented on a self-adhesive foil system. Besides validating the friction reduction it is of high interest to understand the underlying mechanism that causes the reduction. Therefore, a flow channel was designed, that creates a stationary turbulent flow within a square duct allowing for non-invasive measurements by laser doppler velocimetry. The high spatial resolution of the laser device makes recording velocity profiles within the boundary layer down to the viscous sublayer possible. Determination of the wall shear stress τ enables direct comparison of different friction reduction experiments. In this paper we validate the methodology by determining the velocity profile of the flat channel wall (without coatings). We further use the results to validate a CFD model in created in OpenFOAM. We find that velocities along the longitudinal axis are generally in good agreement between numerical and experimental investigations.

1 INTRODUCTION

Friction is a critical factor when it comes to fuel consumption of ships. The lower the friction the lower the energy demand. Therefore, the EU project AIRCOAT¹ aims at reducing hull friction to a minimum. In water ferns, the Salvinia effect of a micro-and nanostructured surface with hydrophobic and hydrophilic characteristics allows for air retention under water [1] and while the air spring effect contributes to the air layer stability [6]. Inspired by the Salvinia effect, the AIRCOAT project intends to develop a biomimetic passive air layer technology.

With a passive air layer covering the hull, the contact area between water and ship is decreased significantly which reduces fuel consumption, carbon dioxide emission as well as acoustic emissions [11, 12]. Water flowing along a solid wall is subject to the no-slip condition with a boundary layer where the fluid velocity increases normal to the surface from zero velocity to freestream velocity [17]. But if the fluid flows along an otherwise liquid or gaseous interface the conditions is expected to differ, which results in friction reduction [10]. To better understand the underlying mechanism of the friction reduction over the hydrophobic AIRCOAT surface, Fraunhofer CML (CML) built a flow channel that creates a stationary turbulent flow driven by hydrostatic pressure. Water is send in a circuit and the test section is a square duct of 40 mm edge length. Made from acrylic glass it allows for noninvasive measurement by a laser

¹ The AIRCOAT project has received funding from the European Union's Horizon 2020 research and innovation programme under grant agreement N°764553.

doppler velocimeter (LDV). The device allows to resolve the boundary layer and the evaluation of the wall shear stress in the boundary layer which is important when it comes to the assessment of wall friction [4]. This study will explain the design and methodology of the flow channel built to perform measurements in a fully developed turbulent flow, the experimental setup and measurements, performed with a non-intrusive LDV device. To further validate the experimental data a comparison with literature is presented. This validation of flow conditions in the test section and measurement technique acts as a prerequisite to perform future measurements with the novel air retaining surface to measure the slip velocities over a hydrophobic wall. In order to better understand the underlying principle of drag reduction, the study further presents a validation of a Computational Fluid Dynamics (CFD) model of the channel. The motivation behind the numerical investigations is crosschecking of the experiments as well as creating a reference for modelling and analysing novel coatings through separate developed wall functions in a Reynolds Averaged Navier Stokes (RANS) simulation.

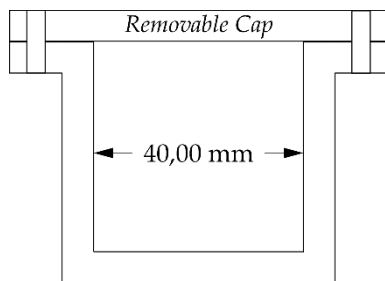


Figure 1. Cross-section of the flow channel duct with removable cap

2 METHODOLOGY

2.1 Channel Setup

The designed flow channel follows a simple and low-cost but effective approach of achieving a fully turbulent flow as well as a fully developed flow profile over the channel height and width. The flow channel setup resembles the setup of [15] and is of a widely adapted setup for this kind of measurement.

The three main features to achieve a fully developed and undisturbed (as much as possible) flow for the presented setup are: 1) a flow induced by hydrostatic pressure with an inflow tank based on an overflow principle to minimise any influence of the pump, which fills the inflow tank, 2) a nozzle in front of the test section specifically designed to minimise flow separation and 3) a test section with a length of 3000 mm and a square cross section of 40.00 mm height and width resulting in the length to height ratio of 75. The flow is driven by a constant water column, which is depicted in the general flow tank setup as vertical pipe in Fig. 2. A constant water

column is guaranteed by the design of the inflow tank, separated into three compartments, with the vertical pipe attached to the centre compartment. Water is pumped into the left compartment, which will spill any excess water into the centre compartment. When the centre compartment is filled, excess water flows into the right compartment. This last compartment is connected to the basin from which the pump is circulating the water back to the inflow tank, i.e. the first compartment. As long as more water is pumped into the elevated inflow tank than is flowing out of the pipes connecting duct and inflow tank, the water column is constant and producing a stationary flow within the test section.

With the flow established, the water is directed into the test section, which is accomplished by using a specifically designed nozzle. Studies have shown that specific geometries reduce the flow separation in nozzles with the best results originating from applying a polynomial of fifth order [18]. This approach has been adapted for the cross-section changing from a circular inflow into the nozzle to a square shaped outflow from the nozzle into the test section. By using additive manufacturing the complex nozzle geometry, depicted in Fig. 2, has been printed and adapted in several iterations to satisfy criteria such as mechanical stability and water tightness. From the nozzle, the flow enters the 3 m long test section where according to [16] fully developed turbulent flow can be expected after passing 70D. The test section is made of acrylic glass and features a removable cover, see Fig. 1. This removable cover allows access over the whole length of the test section. With this key feature it is possible to apply different materials within the duct. In that manner different materials, e.g. the aforementioned foil with hydrophobic properties that can be utilised as ship coating, will be tested regarding friction reduction. The flat and transparent channel walls enable LDV measurements, which is also the main reason for the square cross section. A circular pipe would provide a more preferable environment from a hydrodynamic point of view but would interfere with the laser and cause unwanted refraction and reflections, which again leads to erroneous measurements. Being transparent over the full length there are no limitations to locating the LDV along the flow channel.

2.2 LDV Measurements

With a LDV device it is possible to measure velocity without intruding the flow. The device is mounted perpendicular to the flow channel and the main flow direction and the measurement volume (MV) is oriented normal to the channel wall. The details of LDV principle are well known and described in detail, e.g. in [4]. Within this study the principle is only summarised to explain the basics and why it is a preferable technique for boundary layer assessment based on [2].

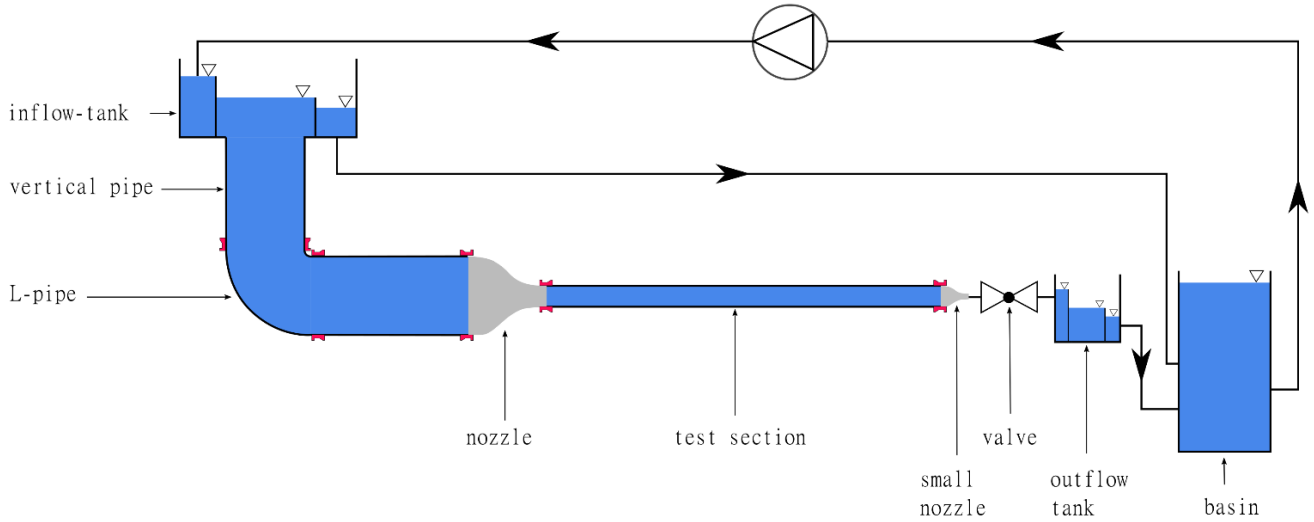


Figure 2. Schematic overview of the flow channel with its main components: inflow tank, vertical pipe to build hydrostatic pressure, L-pipe to direct the flow towards the duct, nozzle with changing cross-section as proposed by [18], test section, small nozzle and valve for flow speed control, outflow tank to regulate water column behind the test section, basin with excess water to feed pump and collect excess water from inflow tank.

$$u = df_D \quad (1)$$

Applying the two Doppler frequencies $f_{D,1}$ and $f_{D,2}$, the velocity of the crossing particle can be determined by Eq. 2. The utilised device has laser beams of wavelength $\lambda_1 = 532$ nm and $\lambda_2 = 561$ nm meeting under an angle of 16 degrees.

$$u_i = \frac{\lambda_i}{2 \sin(\theta/2)} \quad (2)$$

Other than measurements with a conventional LDV, which obtains velocity values for the entire MV, a Profile Sensor allows a higher spatial resolution and the velocity as well as the position of a particle crossing the MV can be obtained. The position, z , of the tracer particle can be determined by the frequency quotient and the calibration function, ϕ , which is provided by the manufacturer [7]. With a known z -position the actual fringe spacing and velocity can be derived [3]. For measurements close to wall - as it is intended in our work to analyse the boundary layer flow - the Profile Sensor is of advantage. The LDV Profile Sensor by ILA R& D [8] offers a spatial resolution up to 1% of the measurement volume length. With a determination of particle positions within the MV the boundary layer, with its linear velocity gradient, can be observed.

$$z = \phi \frac{f_1}{f_2} \quad (3)$$

An LDV device allows only for a quasi-point measurement of flow velocity. Therefore, to record a velocity pattern across the channel height or width multiple measurements need to be performed. After a quasi-point measurement is completed the MV is moved to different location by mechanical traversing and new measurement is started. Afterwards the recorded data from one MV is stitched together to present a flow pattern or near-wall velocity profile.

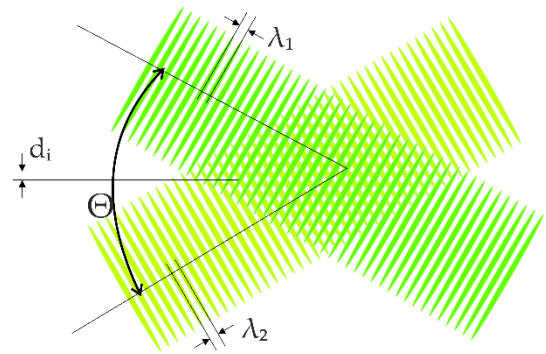


Figure 3. Fringe System of two crossing laser beams. By the combination of two different wave lengths (green areas: λ_1 and λ_2), the known fringe distances d along with a calibration function the velocity and the position of a crossing particle can be calculated. At a particle crossing the MV causes a change in fringe distance and two Doppler frequencies.

3 CFD SIMULATIONS

Table 1. Physical constants for CFD simulation

Quantity	Unit	Value
Density	kg/m ³	998.00
Viscosity	kg/ms	0.001005

In order to quickly transfer experimental results to technical implementation and estimate the performance of surface or hull coatings, e.g. the aforementioned passive air layer, in real world applications, the use of CFD simulations is envisaged. However, to be able to use these tools with confidence, they have to be validated by experimental results. Furthermore, CFD simulations can be used for sanity checks of experimental results. If numerical and experimental results are sufficiently similar it is easier to exclude methodical flaws or systematic measuring errors. Consequently, the internal features of the flow channel described above have been replicated in a Computer Aided Design (CAD) environment to feed into the simulation pipeline.

3.1 Numerical setup

In this study a finite-volume approach is used which utilises the OpenFOAM v1806 package [13]. Only one half of the channel is modelled taking advantage of the symmetry in order to reduce the computational effort. The computational domain is depicted in Fig. 4.

The setup at hand utilises the Reynolds-Averaged-NavierStokes-Equations with $k-\omega$ -SST turbulence model according to [9] to simulate the effects of turbulent flow while limiting the computational effort. Since the flow is gravity driven and assumed to be steady, the *buoyantBoussinesqSimpleFoam* [14] solver and second-order accuracy schemes have been selected. Physical constants were defined according to Table 1.

Due to unknown turbulence properties of the flow at the inlet, initial turbulence parameters were estimated based on the preliminary study and the assumption of fully developed flow with isotropic turbulence at the inlet as given in Table 2. A turbulence parameter study was not conducted as not to distort the validation through false optimisation of input quantities.

Table 2. Initial turbulence parameters

Quantity	Units	Value
κ	m/s ²	1.0070 10 ⁻⁶
ω	s ⁻¹	0.20356
ν	m ² /s	0.01059

3.2 Preliminary study

A preliminary study has been performed to estimate the flow velocities in different parts of the flow channel, namely the vertical pipe, the L-pipe, the nozzle, the test section, the small nozzle and the outflow tank. For this purpose a simple base grid was developed as follows. The maximum cell size was set to 0.011 m. The cell size was halved at the nozzle, which leads into the test section and then halved again for the section stretching from the beginning of the second nozzle through the outflow pipe into the outflow basin. To capture the boundary layer prism cells were applied on the walls. Since the actual local flow velocities were only known for the test section at this stage from the experiments, the thickness of the wall layer was kept constant throughout the domain, which resulted in a variation of y^+ values throughout the domain. However, for estimation of the local velocities this seemed to be sufficient. Fig. 4 shows the magnitude of the velocity in the channel's symmetry plane for the base grid configuration.

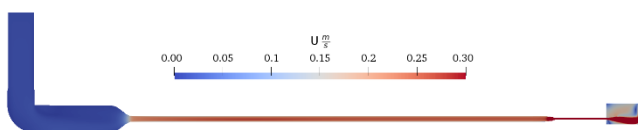


Figure 4. Velocity magnitude in channel symmetry plane, with water flowing from the inlet at the top left into the vertical pipe and onwards into the L-pipe, accelerating inside the nozzle before entering the test section with a maximum velocity of approx. 0.3 m/s, exiting the test section into the second nozzle and finally reaching the outflow tank.

The water enters the inlet at a velocity of about 0.01 m/s and on close inspection flow separation can be spotted on the inside of the sharp 90 degree angle turn inside the L-pipe. The velocity stays approximately constant until it reaches the nozzle before the test section. Moving through the nozzle into the test section, the flow accelerates to close to 0.3 m/s in the centre of the duct. After passing the test section the flow accelerates further in the small nozzle due to the reduction in cross section and exits the outlet pipe into the outlet tank as a distinctive jet.

3.3 Grid study

Based on the results of a preliminary study, a grid study has been performed to study the sensitivity of the results regarding the spatial resolution of the geometry. For this study the maximum cell size was systematically varied by factor of 1.5 to derive one more coarse and two finer grids. The target y^+ was set to ≤ 1 to accurately model the boundary layer which is of prime importance for the planned application of the channel. This means that the number of boundary layer cells varies between the grids. There were no significant differences found between the different grids with volume fluxes, mean and maximum velocities as well as velocity profiles at the 70D position in the experiment found to be in good agreement. The data presented in the following belongs to the grid with a base size of 0.0103 m, which corresponds to the preliminary mesh (base size = 0.011 m) with a minor adjustment to increase the mesh quality to allow for the changes in the boundary layer mesh.

4 RESULTS

4.1 Velocity Patterns of Experiments and Numerical Simulation

Velocity patterns are presented for one longitudinal location along the flow channel at 70D, in which D is the hydraulic diameter of the duct. With the current setup and under given circumstances of chosen equipment the Reynolds number is $Re = 11.400$ in reference to D . The measurements were conducted at one Reynolds number and under the assumption of stationary flow. The normal axis for each pattern is in the centre of the duct for the smallest influence possible by the walls. Presented are velocity patterns across the duct's height, z -pattern, as well as width, y -pattern, in Fig. 5.

The experimental results are 1D measurements and presented are mean values from four measurements. The different markers indicate the z -pattern and y -pattern, respectively. Moreover, an error bar represents the standard deviation for experimental results. The LDV device allows for two parallel measurements at the same time since the two laser beams can record velocities independent from each other, although a measurement event is only valid if the two laser beams detect the same particle. A repetition of that process is performed afterwards. CFD results are presented by dashed and dotted lines, respectively.

From Fig. 5 can be seen that the velocity is symmetric at the respective centre line over the height as well as width, which implies a full turbulent flow. Furthermore, a good agreement with CFD results is clearly visible. Especially the centre line flow shows good agreement for z-pattern as well as y-pattern. Mean velocities are similar to CFD results and the standard deviation for the mean values is small. The measurements closer to the respective channel wall show that turbulence increases and uncertainties of the measurement increase as well. This becomes also visible from the comparison of selected values in experimental data close to the wall. With the different velocities for the points closest to the wall for z-pattern and y-pattern it becomes visible that the experimental data is highly depending on a thorough set-up and fussy alignment of laser device and flow channel.

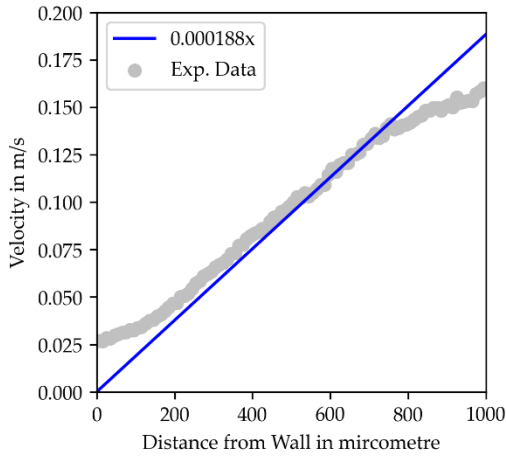


Figure 6. Velocity profile close to the wall with a linear fit (blue line) to determine wall shear stress. The fit curve is forced through zero to imply zero velocity at the wall.

Contrary to CFD results, experimental results do not show zero velocity, since a measurement close to the wall is time consuming and requires high effort. Still, to get an idea of flow conditions a rather coarse measuring grid is sufficient. The comparison shows that the flow at $70D$ is fully turbulent and the respective pattern is nearly symmetric. Furthermore, the y-pattern differs from the z-pattern due to the orientation of the MV that hasn't been changed during the experiments. A measurement to assess the velocities close to the wall, that allow the determination of wall shear stress, is presented in 4.2.

4.2 Near Wall Measurements

A near wall measurement is performed to estimate the possibilities of boundary layer investigations and determination of wall shear stress, τ , within the current channel construction and setup. The MV is located so close to the wall that half the MV is inside the channel and the other half disappearing in the channel wall. After the successful measurement of 10000 particles crossing the MV, the MV is moved step wise away from the wall. Subsequently all recorded MVs are stitched together to build a near-wall flow profile over half the duct ($\delta = 20$ mm). Fig. 6 depicts the near linear increase of velocity between 200 and 800 micrometre wall distance. A linear fit

curve is added to distinguish the intended area. For velocity values further away from the wall, a non-linear gradient becomes visible. Also, clearly visible are the limits of the LDV device, which allows no detection of particles slower than 0.025 m/s (see Sec. 5 for further discussion). Therefore, the linear fit curve is forced to go through zero, since a point directly at the solid wall has zero velocity. The slope of the straight line, or the gradient of the velocity profile near the wall, is assumed to represent the near wall shear stresses from the channel wall [17]. From the relation in Eq. (4), τ can be calculated and can serve as a variable for further boundary layer evaluations with η being the dynamic viscosity of water and $\partial u/\partial y$ the local shear velocity [16]. The determination of τ is highly depending on water carefully recorded velocity and a constant temperature, since small deviations have a strong impact on the result. Fig. 6 indicates room for improvement. Ideally all grey dots would match the blue line.

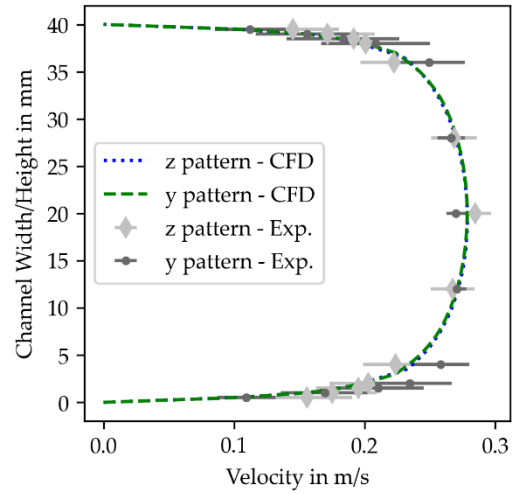


Figure 5. Velocity patterns at $70D$. y pattern is the velocity pattern across the channel width, whereas z pattern is the velocity across the channel height. Horizontal error bars denote the standard deviation of the respective point measurement.

$$\tau = \eta \left. \frac{\partial u}{\partial y} \right|_{y=0} \quad (4)$$

The velocity profile across half the channel duct recorded with a spatial resolution in the near-wall area is presented in Fig. 7, in a semi-logarithmic plot with dimensionless values u^+ over y^+ (with $u^+ = u/u_\tau$ and $y^+ = (y \cdot u_\tau)/\nu$).

From this depiction the non-zero velocity from experimental data becomes visible as well. The blue line represents the area of the linear increase and the green line the log law based on $u^+ = 1/\kappa \cdot \ln(y^+) + C^+$, with $\kappa \approx 0.41$ and $C^+ \approx 5.2$. The logarithmic part of the profile is represented better than the linear portion. This again points out the need for high profoundness in terms of near-wall experiments. Other than that a general agreement between experimental data, theoretical values and literature data, approves the measurement concept and the procedure to determine τ . Although, leaps and irregular values for experimental data implies partly erroneous

measurements. This can be ascribed to the stitching process of the MVs and the recording on different days. Moreover, the determination of wall shear stresses is prone to changes in temperature. This is not considered sufficiently within the selected approach. Nonetheless, the linear part is distinguishable from logarithmic area and therefore determination of slip velocity seems realisable. Results from own numerical calculations are not presented due to the fact that the selected RANS approach uses wall functions. These wall functions are boundary conditions which presume predefined turbulence parameter and velocity profiles normal to the walls, which are derived from the law of the wall. Hence, the compliance to the law of the wall is inherent.

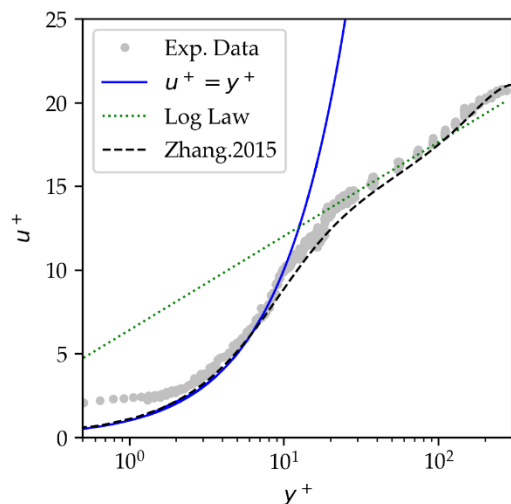


Figure 7. Velocity profile across half the channel duct in comparison with theoretical values and CFD data from [19]. The green line crosses exp. data in the logarithmic layer, whereas the blue line crosses exp. data in the viscous sublayer.

5 CONCLUSION AND OUTLOOK

The general methodology and the proof-of-concept of how to assess the friction reducing capabilities of an air retaining surface were presented. The fundamental principle of the passive air lubrication AIRCOAT surface is to mimic the air retaining properties of the *Salvinia* fern on a foil system, which has both hydrophilic as well as hydrophobic characteristics. One goal of the AIRCOAT project is to prove the friction reducing properties of such an artificial foil in order to validate its potential as a sustainable future ship hull coating. This study serves as the prerequisite for the long term goal to identify and investigate the slip velocity active over a passive air layer. Here, the methodology was validated in a controlled steady environment by investigating a *flat* surface.

The construction of a flow channel driven by a constant water column, the measurement with a LDV Profile Sensor and the implementation of corresponding CFD simulations were reported. The flow channel follows a low-coast approach with the goal of a fully turbulent flow. One Re number was chosen to compare physical experimental results to a CFD simulation. A comparison of experimental data

and CFD results of vertical and horizontal flow patterns showed close resemblance across the square cross-section.

Measurements close to the wall showed the advantage of the LDV Profile Sensor that yielded high resolution measurements within the boundary layer and the near-wall area. The linear increase in velocity, i.e. the local shear velocity, was identified and the mean wall shear stress τ determined.

The performed experiments concluded that well controlled flow conditions and a thorough experimental setup are utterly important to use the full capability of the high spatial resolution achievable with a Profile Sensor, e.g. sturdy construction or temperature monitored fluids.

For future measurements a Profile Sensor with carrier-frequency technique to better identify particles with a near zero velocity is preferable [5]. Such a sensor has the advantage of enabling the determination of flow speeds close to the wall reliably and thus leads to an improved the determination of wall shear stresses.

In future experiments the presented methodology - and validated for *flat* surface with *no air layer* - will be used to assess turbulent flow above a *structured* surface with *air layer* - to identify the velocity profile and the slip velocity. Furthermore, comparing the measured wall shear stress, τ , of *flat* and *structured* surface can give a drag reducing capabilities of passive air retaining surfaces.

Introducing air into the system will bring new challenges. The phase flow regime with the air layer under water will introduce reflection of the laser beam due to different refraction indices of water and air. A reflecting surface is detrimental in achieving a strong LDV measurement signal. Nonetheless, a comparison of these future measurements with the herein presented methodology and reference measurements allow to achieve a valuable contribution in assessing and validating biologically inspired friction reducing ship coatings or surfaces.

The flow channel will further enable the development and validation of custom wall functions for RANS CFD simulations that can subsequently be used to extrapolate the effect of novel coatings such as AIRCOAT to large scales such as ships or the inner walls of pipes and tubes.

ACKNOWLEDGEMENT

The study was performed as part of the AIRCOAT project. The AIRCOAT project has received funding from the European Union's Horizon 2020 research and innovation programme under grant agreement N° 764553. Special thanks goes to Prof. Dr.-Ing. Michael Schlüter and his team from the Institute of Multiphase Flows of the Hamburg University of Technology for giving advise during flow channel design and for lending the LDA Profile Sensor. Furthermore, we thank Prof.(i.R.) Dr. Wolfgang Mackens and his team from the "DLR School Lab" of the Hamburg University of Technology for laboratory access.

REFERENCES

- Barthlott, W., Schimmel, T., Wiersch, S., Koch, K., Brede, M., Barczewski, M., Walheim, S., Weis, A., Kaltenmaier, A., Leder, A., others: The *Salvinia* paradox: superhydrophobic surfaces with hydrophilic pins for air retention under water. *Advanced Materials*. 22, 21, 2325–2328 (2010).
- Boutier, A. ed: *Laser velocimetry in fluid mechanics*. ISTE and Wiley, London and Hoboken, NJ (2012).
- Czarske, J.: Laser Doppler velocity profile sensor using a chromatic coding. *Measurement Science and Technology*. 12, 1, 52–57 (2001). <https://doi.org/10.1088/0957-0233/12/1/306>.
- Czarske, J., Büttner, L., Razik, T., Müller, H.: Boundary layer velocity measurements by a laser Doppler profile sensor with micrometre spatial resolution. *Measurement Science and Technology*. 13, 12, 1979–1989 (2002). <https://doi.org/10.1088/0957-0233/13/12/324>.
- Dues, M., Burgmann, S., Kriegseis, J., Büttner, L., Czarske, J., Janoske, U.: Profilsensormessungen in einem Kanal mit poroerer Wand: Flow-Measurements within a channel with porous wall using laser Doppler profile-sensor. In: *Fachtagung \textquotedblExperiementelle Stroemungsmechanik\textquotedbl*. (2019).
- Gandyra, D., Walheim, S., Gorb, S., Ditsche, P., Barthlott, W., Schimmel, T.: Air Retention under Water by the Floating Fern *Salvinia*: The Crucial Role of a Trapped Air Layer as a Pneumatic Spring. *Small*. 16, 42, 2003425 (2020).
- ILA GmbH: Handbook LDV: LDV system fp50 shift/unshift and software LDA control QT. (2008).
- ILA GmbH: LDV Profile Sensor: ILA Products. (2021).
- Menter, F., Kuntz, M., Langtry, R.B.: Ten years of industrial experience with the SST turbulence model. *Heat and Mass Transfer*. 4, (2003).
- Oeffner, J., Hagemeister, N., Bretschneider, H., Schimmel, T., Jahn, C.: Reducing Friction with Passive Air Lubrication: Initial Experimental Results and the Numerical Validation Concept of AIRCOAT. *Proceedings of HIPER'20: 12th Symposium on High-Performance Marine Vehicles; High-Performance Marine Vehicles*, Cortona, Italy, 12-14 October. 405–417 (2020).
- Oeffner, J., Jalkanen, J.-P., Walheim, S., Schimmel, T.: From nature to green shipping: Assessing the economic and environmental potential of AIRCOAT on low-draught ships. *Proceedings of 8th Transport Research, Arena TRA 2020, April 27-30, 2020, Helsinki, Finland*. (2020).
- Oeffner, J., Weisheit, J., Oikonomou, F., Schimmel, T., Jahn, C.: Biomimetic Self-adhesives Foils instead of Paints: a Business Case for a Sustainable Ship Hull Coating. *Proceedings of 2021 World of Shipping Portugal. An International Research Conference on Maritime Affairs 28-29 January 2021, Online Conference, from Portugal to the World*. (2021).
- OpenCFD Ltd.: *OpenFOAM User Guide*. (2021).
- OpenCFD Ltd.: *OpenFOAM User Guide: A.1 Standard Solvers*. (2021).
- Park, H., Sun, G., Kim, C.-J. "CJ": Superhydrophobic turbulent drag reduction as a function of surface grating parameters. *Journal of Fluid Mechanics*. 747, 722–734 (2014). <https://doi.org/10.1017/jfm.2014.151>.
- Pope, S.B.: *Turbulent flows*. Cambridge Univ. Press, Cambridge (2000).
- Schlichting, H., Gersten, K., Krause, E.: *Grenzschicht-Theorie*. Springer, Berlin (1997).
- Zanoun, E.-S.: Flow characteristics in low-speed wind tunnel contractions: Simulation and testing. *Alexandria Engineering Journal*. 57, 4, 2265–2277 (2018). <https://doi.org/10.1016/j.aej.2017.08.024>.
- Zhang, H., Trias, F.X., Gorobets, A., Tan, Y., Oliva, A.: Direct numerical simulation of a fully developed turbulent square duct flow up to. *International Journal of Heat and Fluid Flow*. 54, 258–267 (2015). <https://doi.org/10.1016/j.ijheatfluidflow.2015.06.003>.